MINERALOGIA, *40, No. 1–4: 95–106 (2009)*
DOI: 10.2478/v10002-009-0008-x
www.Mineralogia.pl

MINERALOGICAL SOCIETY OF POLAND
POLSKIE TOWARZYSTWO MINERALOGICZNE

Short note

Characterization of granites by ^{57}Fe Mössbauer spectroscopy

Kamaledin M. HASSAN[1]

[1] *Nuclear Materials Authority, P.O. Box 530, Maadi, Cairo, Egypt: email: egy100@yahoo.com*

Received: November 30, 2009
Received in revised form: March 5, 2010
Accepted: March 15, 2010
Available online: March 30, 2010

Abstract. Two granite complexes in Egypt, a sodic type and an aluminous type are characterized by Mössbauer spectroscopy. Mössbauer spectra (MS) of the sodic granite show a major doublet of ferric (Fe^{3+}) iron that is attributable to octahedral coordination (M1) sites plus/minus a tetrahedron Fe^{3+} doublet plus/minus a doublet of ferrous (Fe^{2+}) iron on the M1 sites plus/ minus another Fe^{2+} (M1) doublet and a sextet of Fe^{3+}. The sextet is attributed to α-Fe_2O_3 (hematite) and the other Fe components are due to $NaCaFeSi_2O_6$ (aegirine-augite) plus/minus minor contributions from $(Ca_2(Mg,Fe)_5(Si,Al)_8O_{22}(OH)_2$ (magnesium-hornblende). Changes in the quadrupole splitting and width line of Fe^{2+} ions are likely composition-related. The MS of the aluminous-type granite, on the other hand, shows evidence only of single doublets containing Fe^{2+} or Fe^{3+} in the octahedral M1 sites, with parameters that remain almost constant. This consistency implies that the existing minerals – $K(Mg,Fe^{2+})_3$ $(Al,Fe^{3+})Si_3O_{10}(OH,F)_2$ (biotite), $(Mg,Fe)_6(Si,Al)_4O_{10}(OH)_8$ (clinochlore), $(Na,K)Ca_2(Fe,Mg)_5(Al,Si)_8O_{22}(OH)_2$ (ferrohornblende and magnesiohornblende) – have similar iron positions. The intensity of iron oxidized ($Fe^{3+}/\Sigma Fe$) for the sodic granite is 79.1 to 100% and for the aluminous granite, 28.4 to 38.2%. The observed $Fe^{3+}/\Sigma Fe$ differences between the two granites are source-related and consistent with distributions of other redox-sensitive elements.

Key-words: granitic types, clinopyroxene, mica, amphibole, Mössbauer spectroscopy, oxygen fugacity, Western Desert

1. Introduction

Iron (^{57}Fe) Mössbauer spectroscopy provides information regarding iron in a solid structure as to its oxidation state (e.g. Fe^{3+}, Fe^{2+}), coordination type (e.g. tetrahedral, octahedral) and relative order (regular vs. distorted) for each iron-occupied site in the sample (see Kuzmann et al. 2003, for a thorough review). In contrast to X-ray diffraction, it also provides information on compounds with poor crystallinity and/or low concentrations; for example, iron oxides such as

hematite and aluminous hematite in granitic soils are easily distinguished from each other and from Fe in layer silicates (Hassan 2008a). In addition, the relative intensities of the various identified peaks reflect the relative concentrations of compounds in the samples and can be used in a semi-quantitative analysis. Results obtained from ^{57}Fe Mössbauer spectroscopy are independent of composition: the gamma (γ)-rays emitted by ^{57}Co are sensitive only to ^{57}Fe in a sample. Furthermore, this method does not depend on chemical analyses for calibration.

Because ^{57}Fe Mössbauer spectroscopy enables measuring changes in the electronic-, magnetic-, geometric-, or defect structure as well as in the lattice vibrations in Fe-bearing solids, it provides a unique probe for studying the variations of iron sites in a large variety of granite rocks (Bahgat, Hassan 1988; Eissa et al. 1994a, b). In the present study, the technique has been applied to the bulk chemistry of a sodic granite and to an aluminous granite located ~100 kilometers apart in the Nubian Sand in the south Western Desert, Egypt (Fig. 1). This study is particularly important in the assignment of the oxidation states of iron and in the identification of hematite, which are parameters of considerable geological importance in the evaluation of these rocks and their environments.

An account of the geological settings, ground radiometric and geochemical characteristics of the two granite types is given by Hassan (2005, 2008b).

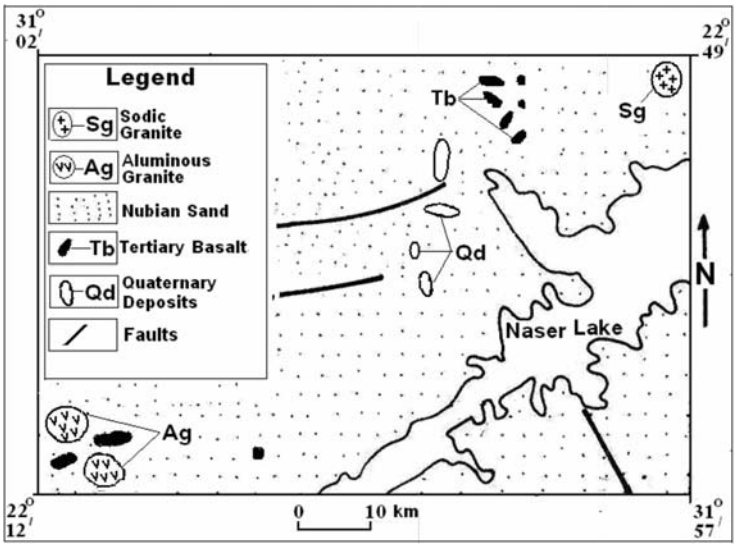

Fig. 1. Geological map of south Western Desert, Egypt
(revised from Egyptian Geological Survey and Mining Authority, 1981)

2. General characterization of granites

2.1. Sodic granite

The sodic granite, a prospective environment for uranium, thorium, relatively rare elements, and rare earths, crops out as a ring-like feature (area ≈ 9 km^2) comprising homogenous granite

cut by a few peralkaline dykes and consisting of quartz, feldspars and brown to green-colored clinopyroxenes. It may be classified under the so-called "g_γ" granites, a variety of quartz syenites and granitiods having a peralkaline tendency and often found in ring complexes and dike-like intrusions from the end of Precambrian to the Paleozoic in Egypt (List et al. 1989). Characteristically, this granite possess a high level of total field γ- radiation, up to 1800 counts per second (cps), in devitrified glasses along shear zones but without any obvious radioactive mineralization. The radiation is due to thorium and, to a lesser extent, uranium. The radioactive elements reside in trace mineral phases and also in iron compounds.

2.2. Aluminous granite

The aluminous granite, occurring in the form of isolated knobs and residual boulders (area ≈ 20 km^2) with low γ-ray intensities (80–250 cps), contains dark brown micas (biotite) and amphiboles. These granite forms, which differ in composition and texture, are the remnants of a mountain that succumbed to desert erosion which is evident from the abundant granite debris and soils in the surroundings (Hassan 2008b). According to Sabet (1972), the aluminous granite may be linked to the tonalite-granodiorite magma, emplaced in successive phases containing biotite, hornblende or both during the Proterozoic in Egypt.

3. Methods

Ten representative samples, six (S1 to S6) of the sodic granite and four (A1 to A4) of the aluminous granite were examined. Different samples were previously analyzed for major and minor elements (Hassan 2005, 2008b). The chemical results and calculated values of the peralkalinity index (PI = mol $Na_2O + K_2O/Al_2O_3$) and the aluminum saturation index [ASI = mol $Al_2O_3/ Na_2O + K_2O + CaO$] are given in Table 1. Samples S1 to S6, with values of PI > 1, are peralkaline. Samples A2 and A3 are peraluminous (PI < 1 and ASI > 1) while samples A1 and A4 are metaluminous (PI < 1, ASI < 1). Sodic granite samples contain up to: 16 ppm U, 37 ppm Th, 45 ppm Y, 656 ppm Zr, 54 ppm Nb, 533 ppm Ce, 41 ppm Sm and 452 ppm Nd. Aluminous granite samples, in contrast, have lesser contents of: U (0.7–3.7 ppm), Th (0.2––2.6 ppm), Zr (115 ppm), Nb (4–7 ppm) and Y (8 ppm).

Powder X-ray diffraction analysis of the samples was obtained using a Philips PW 1710 diffractometer. Examples of X-ray diffractograms with the identification of minerals are shown in Figure 2. In the sodic granite, besides quartz and feldspars, aegirine-augite was identified as the major iron component: it is associated with minor amounts of magnesiohornblende in S2, S3, S4 and S5. In the aluminous granite, three different iron mineralogies were recognized. These are: (1) biotite plus some magnesiohornblende with minor clinochlore in A1 and A2, (2) ferrohornblende plus some clinochlore in A3 and (3) magnesiohornblende plus some biotite with minor clinochlore in A4.

Mössbauer measurements were performed on the bulk fraction of heavy minerals that was separated from crushed granite samples with bromoform. Aliquots of the bulk heavy fraction (150 mg) were mixed with sugar and then milled together to obtain the finest texture possible. Mössbauer spectra were obtained using a multichannel analyzer (1024 channels) operated with

TABLE 1

Chemical composition of the sodic and aluminous granites (after Hassan 2005 and 2008b)

Sample	Sodic granite						Aluminous granite			
	S1	S2	S3	S4	S5	S6	A1	A2	A3	A4
					(wt%)					
SiO_2	67.0	70.0	73.0	71.7	66.0	70.0	65.5	69.0	72.7	55.5
Al_2O_3	70.4	8.40	9.2	2.60	–	4.30	13.3	12.8	12.8	12.8
CaO	1.00	1.96	0.86	2.89	0.40	2.10	2.18	1.00	0.26	3.50
Na_2O	4.60	1.88	3.90	4.90	3.92	4.82	3.80	3.36	4.03	5.04
K_2O	3.97	5.90	4.60	1.45	3.72	3.67	4.23	3.30	3.27	2.73
					(ppm)					
Th	37	27	23	24	–	–	1.4	2.6	2.7	0.2
U	16	10	13	16	–	–	1.8	0.7	3.7	1.1
Rb	131	145	–	–	–	–	77*	–	76*	–
Sr	7	24	–	–	–	–	198*	–	87*	–
Y	45	31	–	–	–	–	8*	–	4*	–
Zr	656	442	–	–	–	–	115*	–	53*	–
Nb	54	24	–	–	–	–	7*	–	2*	–
Ba	1604	783	–	–	–	–	1379*	–	243*	–
Ce	533	241	–	–	–	–	–	–	–	–
Sm	41	16	–	–	–	–	–	–	–	–
Nd	360	452	–	–	–	–	–	–	–	–
					Chemical Indices					
PI	1.61	1.13	1.24	3.64	–	2.77	0.82	0.71	0.79	0.88
ASI	0.54	0.64	0.71	0.17	–	0.27	0.90	1.17	1.2	0.73

Dash: not analyzed; S1-6, A2 (coarse-grained granite); A1 (medium-grained grandiorite); A3 (fine-grained gneissose granite); A4 (equigranular monzodiorite);

* New analysis using X-ray fluorescence method.

an electromechanical drive system with a symmetric triangular velocity shape. During the experiments, the source (25 m Ci ^{57}Co/Rh) and absorber were kept at room temperature (298 K). The spectra obtained were fitted by computer to Lorentzian line shapes in order to obtain accurate line parameters.

4. Results and discussions

The Mössbauer parameters of the sodic granite spectra are summarized in Table 2 and the computer-fitted plots of three representative spectra are given in Figure 3. Each spectrum has a major, narrowly split, asymmetric ferric doublet (D1). According to Amthauer, Rossman

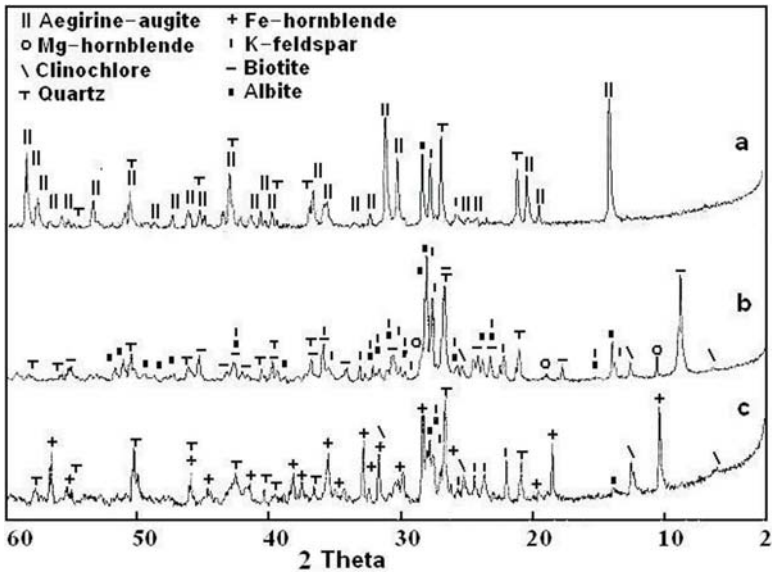

Fig. 2. X-ray diffraction patterns of the samples: S1 (a), A2 (b), and A3 (c)

TABLE 2

Mössbauer hyperfine parameters of the sodic granite samples at room temperature

Sample	H[a]	ΔE_Q[b]	δ[c]	Γ[d]	RA[e]	Interpretation	
						Iron site	Iron mineralogy
S1	–	0.29	0.40	0.32	84.7	D1: Fe^{3+} (M1)	aegirine-augite
	–	0.15	0.25	0.42	15.3	D2: Fe^{3+} (T)	aegirine-augite
S2	–	0.31	0.37	0.37	92.6	D1: Fe^{3+} (M1)	aegirine-augite + minor Mg-hornblende
	–	2.70	1.15	0.65	7.40	D3: Fe^{2+} (M1)	aegirine-augite + minor Mg-hornblende
S3	–	0.34	0.38	0.41	85.1	D1: Fe^{3+} (M1)	aegirine-augite + minor Mg-hornblende
	–	2.66	1.18	0.49	14.9	D3: Fe^{2+} (M1)	aegirine-augite + minor Mg-hornblende
S4	–	0.35	0.40	0.34	79.1	D1: Fe^{3+} (M1)	aegirine-augite + minor Mg-hornblende
	–	2.55	1.17	0.59	20.9	D3: Fe^{2+} (M1)	aegirine-augite + minor Mg-hornblende
S5	–	0.32	0.39	0.34	60.8	D1: Fe^{3+} (M1)	aegirine-augite + minor Mg-hornblende
	–	2.13	1.19	1.13	13.8	D4: Fe^{2+} (M1)	aegirine-augite + minor Mg-hornblende
	50.9	–0.21	0.38	0.36	25.4	HFD: Fe^{3+}	hematite
S6	–	0.29	0.40	0.33	71.9	D1: Fe^{3+} (M1)	aegirine-augite
	–	2.05	1.07	0.89	8.70	D4: Fe^{2+} (M1)	aegirine-augite
	50.9	–0.20	0.38	0.56	19.4	HFD: Fe^{3+}	hematite

H[a] = hyperfine magnetic field; ΔE_Q[b] = quadrupole splitting; δ[c] = isomer shift; Γ[d] = width line; RA[e] = relative area. The values of H are in tesla (T); those of δ, ΔE_Q and δ in millimeters per second (mm/s); and RA in percent (%). Errors on H are roughly ± 0.6 T; for ΔE_Q, δ and Γ roughly ± 0.04 mm/s, and for RA ± 1.66–2.22%. All δ values are relative to metallic iron.

(1984), the asymmetry of D1 is due to relaxation effects. It is well established that these effects induce an asymmetric feature in aegirine over a wide range of temperatures up to 480 K (De Grave et al. 1998). Another ferric doublet (D2) that is extremely narrow and symmetric was identified only in the spectrum of S1 (Fig. 3a). A symmetric, wide-spaced doublet of ferrous (D3) seen in the spectrum of S3 (Fig. 3b) is representative of similar features in S2 and S4. Another ferrous doublet (D4) plus a sextet due to a hyperfine field distribution (HPD) phase, are recognized in the spectrum of S5 (Fig. 3c) and, identically, in S6.

D1, with relative spectral areas or RA values of 60–85%, has quadrupole splitting (ΔE_Q) and isomer shift (δ) varying from 0.29–0.35 and from 0.37–0.40 mm/s, respectively. The values of ΔE_Q and δ are consistent with Fe^{3+} in octahedral (M1) coordinations and agree with those reported for aegirine (Hassan 2009; De Grave et al. 1998; Dollase, Gustafson 1982) and aegirine-augite (Baum et al. 1997). Aegirine-augite is an intermediate member of the aegirine ($NaFe^{3+}Si_3O_8$)-augite ($(Ca,Mg,Fe)SiO_3$) series. In this series, the Na^+ is partially replaced by Ca^{2+} with Fe^{2+} and Mg^{2+} replacing the Fe^{2+} to balance the charge; these ionic processes cause localized distortion of the electron cloud at the ferric site and, thus, increases its quadrupole

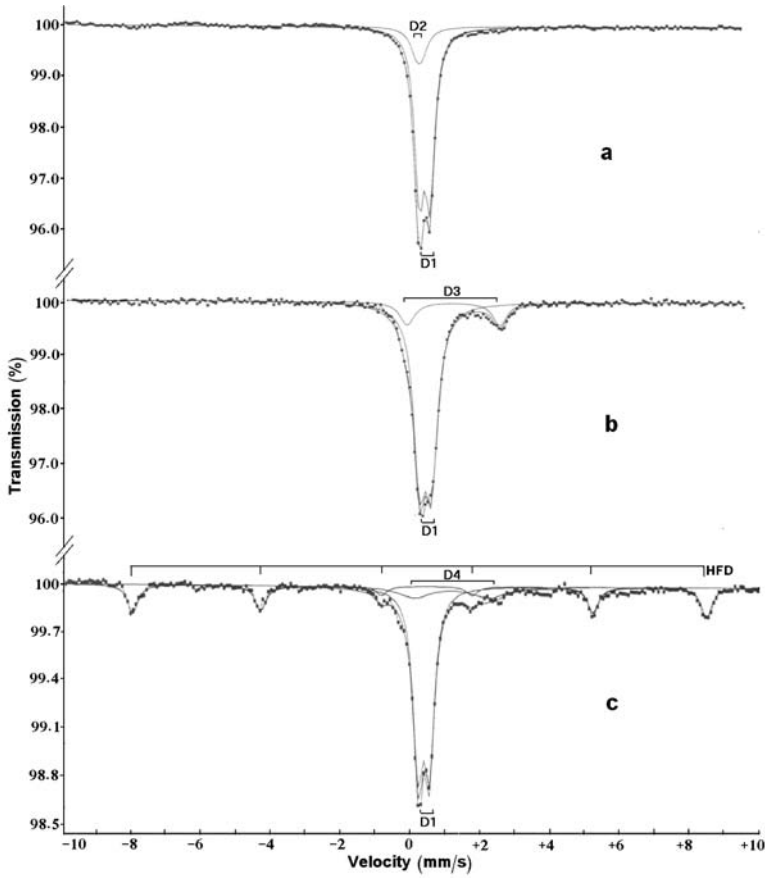

Fig. 3. Mössbauer spectra of the samples S1 (a), S3 (b) and S5 (c),
giving a representative picture of the differences found by Mössbauer analysis for the studied sodic granite

splitting. Therefore, the overall variation (0.06 mm/s) in the ΔE_Q values may be due to a small amount of ionic exchange. This variation is also expected as the sodic granite (except for samples S1 and S6) does not contain only a single Fe mineral phase (aegirine-augite) but variable minor amounts of magensiohornblende.

The D2 spectrum with a relative spectral area of ~ 15% is characterized by $\Delta E_Q = 0.15$ mm/s and $\delta = 0.25$ mm/s. These characteristics, according to other published data (De Grave 1998; Akasaka 1983; Dyar et al. 2004), reflect a tetrahedron (T) coordination. The D3 and D4, with RA values between 7.4 and 20.9%, are characterized by different parameters. ΔE_Q values of D3 vary from from 2.55 to 2.70 mm/s while those for D4 from 2.05–2.13 mm/s. The δ values vary from 1.15–1.18 mm/s in D3 and from 1.07–1.19 mm/s in D4. Variations in the ΔE_Q and δ values could result from differences in the Fe mineralogy and/or as a result of ionic exchange processes. These variations are consistent with Fe^{2+} in M1 sites in aegirine-augite and also agree within experimental error with values reported by Goldman (1979) for amphibole minerals. In general, amphiboles, pyroxenes and micas contain Fe^{2+} in octahedral coordination, and thus have very similar Mössbauer parameters.

The hyperfine field distribution (HFD) site with an asymmetric sextet line characterized by $\Delta E_Q \sim -0.21$ mm/s and $\delta = 0.38$ mm/s represents hematite. Its hyperfine field or (H) ~ 50.9 tesla is slightly lower than that of well-crystallized and chemically pure hematite (Fysh, Clark 1982), but may be attributed to the presence of Ti^{4+} (Dyar et al. 2004) or Al^{3+} (Hassan 2008a), which would depress the hyperfine field. This hematite sextet would not be compatible with two subcomponents/sextets and, therefore, the presence of other hyperfine phases is ruled out. The identified hematite has a relative spectral area of ~ 19% in S6 to ~ 25% in S5 (Table 2). Despite its considerable intensity in these two samples, hematite was difficult to confirm using X-ray diffraction. In general, iron oxides formed under high states of oxidation and/or radioactivity (particularly α-radiation) do not exhibit long-range order: such materials are difficult to study by XRD but are easily identified by Mössbauer spectroscopy mainly on the basis of their magnetic properties.

A noteworthy feature in Table 2 is that the line widths (Γ values) for D1 and D2 are >0.50 mm/s > D3 and HFD fall in the range 0.36–0.65 mm/s and D4 exhibits a considerable line broadening, from 0.89–1.13 mm/s. Although it proved impossible to resolve closely overlapping peaks, their breadth is indicative of ions of different valences being located in more than one site in the mineral structure. Line broadening has been reported for Fe^{2+} in aegirine and attributed to hopping (electron exchange) between the adjacent Fe^{2+} and Fe^{3+} sites (Amthauer, Rossman 1984). This process increases with increasing cation substitution; this is evident from the changes of the ΔE_Q values for D3 and D4.

Unlike the sodic granite spectra, those of the aluminous granite and their fits are nearly identical. All consist of a widely-spaced doublet due to Fe^{2+} and a narrow one due to Fe^{3+}, both of which are in octahedral M1 sites. The spectrum for S4 is given as an example in Figure 4. As shown in Table 3 sample A4 has the lowest Fe^{2+}/Fe^{3+}. This ratio ranges from 1.62 in A4 to 2.52 in A3, these are two samples that contain different Fe minerals (magnesiohornblende and biotite plus some clinochlore in A4, ferrohornblende plus some clinochlore in A3). The Fe^{2+} has ΔE_Q from 2.56–2.58 mm/s and δ from 1.13–1.16 mm/s, wheras the Fe^{3+} has values of 0.71–0.75 mm/s, and 0.49–0.50 mm/s, respectively. The relative consistency of the ΔE_Q and δ values, despite the considerable change of iron mineralogy, suggests that the minerals present

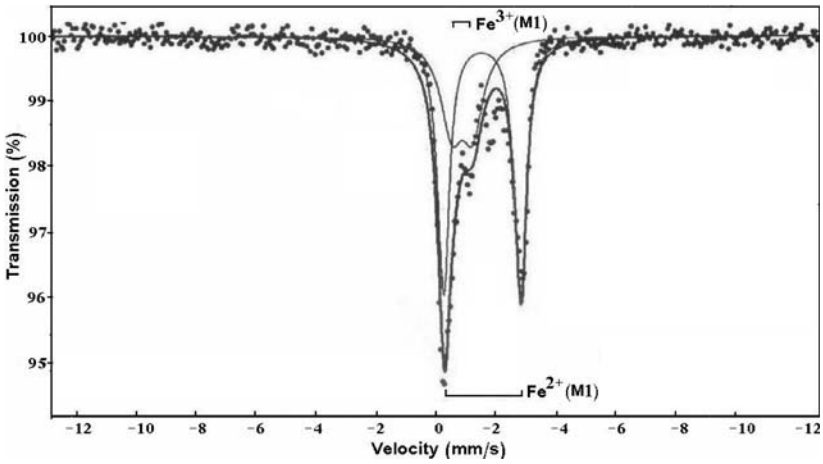

Fig. 4. Mössbauer spectrum of sample A2 is typifying the studied aluminous granite

TABLE 3

Mössbauer hyperfine parameters of the aluminous granite samples measured at room temperature

Sample	Fe^{2+} M1				Fe^{3+} M1				$\frac{Fe^{2+}}{Fe^{3+}}$	Iron mineralogy (minor phases in parentheses)
	ΔE_Q	δ	Γ	RA	ΔE_Q	δ	Γ	RA		
A1	2.56	1.15	0.42	64.5	0.73	0.50	0.67	35.5	1.82	biotite, (Mg-hornblende)
A2	2.58	1.14	0.41	62.9	0.71	0.50	0.62	37.1	1.70	biotite, (Mg-hornblende)
A3	2.59	1.13	0.44	71.6	0.75	0.49	0.63	28.4	2.52	Fe-hornblende, (clinochlore)
A4	2.59	1.16	0.48	61.8	0.71	0.50	0.31	38.2	1.62	Mg-hornblende, biotite, (clinochlore)

have iron in similar sites: they cannot be discriminated by their Mössbauer spectral data alone. This agrees with previous studies, indicating MS similarities among various rock-forming minerals including biotite (Fe^{2+} ΔE_Q = 2.59 mm/s, Fe^{2+} δ = 1.13 mm/s; Fe^{3+} ΔE_Q = 0.75 mm/s; Fe^{2+} δ = 0.45 mm/s; Macedo et al. 1994), hornblende (Fe^{2+} ΔE_Q = 2.59 mm/s; Goldman 1979) and chlorite (Fe^{2+} ΔE_Q = 2.63 mm/s, δ = 1.15; Fe^{3+} ΔE_Q = 0.80 mm/s, δ = 0.40 mm/s; Coey 1975).

In Table 4, a comparison is made between the two granites on the basis of $Fe^{3+}/\Sigma Fe$ determined directly from the RA values (Tables 2 and 3). Values of $Fe^{3+}/\Sigma Fe$ in sodic granite range from 79.1–100% and average 89.1%. The $Fe^{3+}/\Sigma Fe$ values in aluminous-type granite range from 28.4–38.2 and average 34.8%. The range of $Fe^{3+}/\Sigma Fe$ values for the sodic granite exceeds the average range (56.04%) of peralkaline granites with riebeckite (sodic amphibole) as the major iron mineral (Hassan and Abu Anbar 1997; Khalaf et al. 1994, 2000). The range of

TABLE 4

Mössbauer determination of the oxidized iron ratio in the samples studied

Rock type	Sample	($Fe^{3+}/\Sigma Fe$) [%]
Sodic granite	S1	100
	S2	92.6
	S3	85.1
	S4	79.1
	S5	86.2
	S6	91.3
	Average	89.1
Aluminous granite	A1	35.5
	A2	37.1
	A3	28.4
	A4	38.2
	Average	34.8

$Fe^{3+}/\Sigma Fe$ values for the aluminous granite, on the other hand, is typical of metaluminous to weakly peraluminous A-type granites (King et al. 1997; Whalen et al. 1987). The peralkaline granites and the metaluminous to weakly peraluminous A-type granites are two distinctive types and likely evolved under different redox conditions (oxygen fugacities).

Oxygen fugacity (f_{O_2}) refers to the activity (partial pressure) of O_2 within a system. The f_{O_2} is a critical factor during the evolution of igneous rocks because it controls the proportions of Fe^{2+} and Fe^{3+} in melts. However, the f_{O_2} impact on Fe^{3+}/Fe^{2+} in a geological system is complicated by temporal and spatial variations in the temperature and pressure of the system, heterogeneous composition (Kress, Carmichael 1991) and quenching conditions (Dyar et al. 1987). High charge-to-radius cations tend to increase Fe^{3+}/Fe^{2+}, whereas low charge-to-radius cations decrease Fe^{2+} (Dyar 1985). In minerals, Fe^{3+}/Fe^{2+} is a function of crystal chemistry and the f_{O_2} during crystallization (McCanta et al. 2003). Olivine, for example imposes limits on the amount of Fe^{3+} which can be incorporated in its structure and may not, therefore, regularly record changes in magmatic f_{O_2}. Another example, the sodic-amphibole (arfvedsonite), is chemically unstable and alters to aegirine (Marks et al. 2003; Salvi, William-Jones 2006) and, hence, its Fe^{3+}/Fe^{2+} ratio may not reflect the intrinsic f_{O_2} of the source magma. However, the chemistry of iron in clinopyroxene tends to be steady which, thus, makes it a potential oxybarometer (McCanta et al. 2004). The stability of clinopyroxenes (mainly aegirine) is evident in old geological records (Marks et al. 2003). Therefore, the elevated $Fe^{3+}/\Sigma Fe$ values of the sodic granite are likely primary and to reflect high states of f_{O_2}. On the other hand, the aluminous granite with consistently low $Fe^{3+}/\Sigma Fe$ values might reflect low f_{O_2} conditions. These assessments are also consistent with the high contents of uranium, thorium, zirconium, niobium and yttrium in sodic-type samples compared to the aluminous-type samples. These elements, like iron, are f_{O_2}-dependent and their distributions provide an indication of the redox conditions of formation.

In conclusion, the Mössbauer parameters of the granites studied have been analyzed, with their possible utilization in mind. The application of these data have been found to separate the sodic- and aluminous granite types, and to reveal particulars of their formation. This study is of importance from both a theoretical and practical point of view, since the granites occur in very different geochemical associations and the sodic granite, formed under highly oxidized conditions, contains a relatively high level of radioactive and rare metals.

Acknowledgements. The author acknowledges the staff of the "Toshki Uranium Study and Evaluation Project" for their field assistance, Professor I. Kashif and Professor S.S. Ata-Allah for Mössbauer analyses. Special thanks to the reviewers who aided in clarifying some of the arguments presented in this paper.

5. References

Akasaka M. (1983). ^{57}Fe Mössbauer study of clinopyroxenes in the join $CaFe^{3+}AlSiO_6$–$CaTiAl_2O_6$. *Physics and Chemistry of Minerals*, 9, 205–211.

Amthauer G., & Rossman G.R. (1984). Mixed valence of iron in minerals with cation clusters. *Physics and Chemistry of Minerals*, 2, 119–154.

Bahgat A.A., & Hassan K.M. (1988). Mixed valent iron in biotite. *Hyperfine Interactions*, 41, 755–758.

Baum E., Treutmann W., Lottermoser W., & Amthauer G. (1997). Magnetic properties of the clinopyroxenes aegirine and hedenbergite: a magnetic susceptibility study on single crystals. *Physics and Chemistry of Minerals*, 24, 294–300.

Coey J.M.D. (1975). The clay minerals: use of Mössbauer spectroscopy to characterize them and study their transformations. Proceedings – International Conference on Mössbauer Spectroscopy, August 25–30 (pp. 333–353). Cracow, Poland.

De Grave E., Van Alboom A., & Eeckhout S.G. (1998). Electronic and magnetic properties of a natural aegirine as observed from its Mössbauer spectra. *Physics and Chemistry of Minerals*, 25, 378–388.

Dollase W.A., & Gustafson W.I. (1982). Mössbauer spectral analysis of the sodic clinopyroxenes. *American Mineralogist*, 67, 311–327.

Dyar D.M. (1985). A review of Mössbauer data on inorganic glasses: the effects of composition on iron valency and coordination. *American Mineralogist*, 70, 304–316.

Dyar M.D., McEnroe S.A., Murad E., Brown L.L., & Schiellerup H. (2004). The relationship between exsolution and magnetic properties in hemo-ilmenite: Insights from Mössbauer spectroscopy with implications for planetary magnetic anomalies. Geophysical Research Letters, 31, L04608. DOI: 10.1029/2003GL019076.

Dyar D.M., Naney M.T., & Swanson S.E. (1987). Effects of quench method on Fe^{3+}/Fe^{2+} ratios: a Mössbauer and wet-chemical study. *American Mineralogist*, 72, 792–800.

Egyptian Geological Survey and Mining Authority. (1981). *Geological map of Egypt, scale 1:2,000,000*. Abbasyia, Cairo, Egypt: Geological Survey and Mining Authority.

Eissa N.A., Sallam H.A., & El Bahnassawy H.H. (1994a). Mössbauer study of Egyptian granite. *Arab Journal of Nuclear Sciences and Applications*, 27, 87–96.

Eissa N.A., Abou Sehly A.A., Shash N., Salman F., & El Bahnassawy H.H. (1994b). Mössbauer spectra electrical and thermal conductivities of Egyptian granite. *Arab Journal of Nuclear Sciences and Applications*, 27, 109–126.

Fysh S.A., & Clark P.E. (1982). Aluminous hematite. *Physics and Chemistry of Minerals*, 8, 257–267.

Goldman D.S. (1979). A reevaluation of the Mössbauer spectroscopy of calcic amphiboles. *American Mineralogist*, 64, 109–119.

Hassan K.M. (2005). Geochemical assessment of radioactive lava pockets in El-Seboah granite, Toshki area, south Western Desert, Egypt. *Annals of the Geological Survey of Egypt*, XXVIII, 195–204.

Hassan K.M. (2008a). Characterization of granitic soil samples from Egypt by ^{57}Fe Mössbauer spectroscopy. *Isotope and Radiation Research*, 40, 107–116.

Hassan K.M. (2008b). Petrography, chemistry and radioactivity of granitoids at north Gebel Seri, south Western Desert, Egypt. *Isotope and Radiation Research*, 40, 615–629.

Hassan K.M. (2009). Rhyolite-dacite-trachyandesite association: a Mössbauer spectroscopy study. Hyperfine Interactions, 192, 101–107.

Hassan A.M., & Abu Anbar M.A. (1997). Geochemistry and mineral chemistry of some alkalic granites of Egypt. Proceedings – International Conference on Geochemistry of igneous rocks and geochemical exploration, September 3–4 1997 (pp. 121–127). Alexandria, Egypt.

Khalaf I.M., Ahmed A.M., & Sewifi B.M. (1994). The granitoids of Ras Muhammad area, south Sinai, Egypt. *Egypt Journal of Geology*, XXXVIII, 125–139.

Khalaf I.M., Abdel Monem A.A., Attawiya Y.M., Ammar S.E., & El-Sawey E.H. (2000). Petrology, geochemistry and radioactivity of Abu Aqarib Alkali granite, Central-Eastern Desert, Egypt. *Annals of the Geological Survey of Egypt*, 38, 261–274.

King P.J., White A.J.R., Chappell B.W., & Allen C.M. (1997). Characterization and origin of aluminous A-type granites from the Lachlan Fold Belt, Southeastern Australia. *Journal of Petrology*, 38, 371–391.

Kress V.C., & Carmichael I.S.E. (1991). The compressibility of silicate liquids containing Fe_2O_3 and the effect of composition, temperature. Oxygen fugacity and pressure on their redox states. *Contributions to Mineralogy and Petrology*, 108, 82–92.

Kuzmann E., Nagy, S., & Vértes A. (2003). Critical review of analytical applications of Mössbauer spectroscopy illustrated by mineralogical and geological examples. *Pure Applied Chemistry*, 75, 801–858.

List F.K., El-Gaby S., & Tehrani R. (1989). The basement rocks in the Eastern and Western Deserts and Sinai. In M. Hermina, E., Klitzsch & S. List (Eds.), *Stratigraphic lexicon and explanatory note to the geologic map of Egypt 1:500000* (pp. 33–56). Cairo, Egypt: Egyptian General Petroleum Corporation.

Macedo W.A.A., Mariano V.R.P.R.O., Correia Neves J.M., & Svisero D.P. (1994). Mössbauer characterization of biotites from zoned pegmatites. *Hyperfine Interactions*, 83, 483–487.

Marks M., Vennemann T., Siebel W., & Markl G. (2003). Quantification of magmatic and hydrothermal processes in a peralkaline syenite-alkali granite complex based on textures, phase equilibria, and stable and radiogenic isotopes. Journal of Petrology, 44, 1247–1280.

McCanta, C., Rutherford, M.D., Dyar, M.D., & Delaney, J.S. (2003). Fe^{3+}/?Fe ratios in pigeonite as a function of f_{O_2}: a preliminary investigation. Proceedings – XXXV Lunar and Planetary Science Conference, Abstract 1361.

McCanta C., Rutherford M.D., Dyar M.D., & Delaney J.S. (2004). The relationship between clinopyroxene Fe^{3+} content and oxygen fugacity. Proceedings – XXXV Lunar and Planetary Science Conference, Abstract 1198.

Sabet A.H. (1972). On the stratigraphy of basement rocks of Egypt. *Annals of the Geological Survey of Egypt*, II, 79–102.

Salvi S., & William-Jones A.E. (2006). Alteration, HFSE mineralization and hydrocarbon formation in peralkaline igneous systems: Insights from the Lake Strange Pluton, Canada. *Lithos*, 91, 19–34.

Whalen B. J., Currie L.K., & Chappell W.B. (1987). A-type granite: geochemical characteristics, discrimination and petrogenesis. *Contributions to Mineralogy and Petrology*, 95, 407–419.